Theoretical study of evaporation-residue cross sections for fusion reactions at energies near the Coulomb barrier

Bing Wang (王兵) ●,* Zi-Yang Yue (岳子洋), and Wei-Juan Zhao (赵维娟)
School of Physics and Microelectronics, Zhengzhou University, Zhengzhou 450001, China

The empirical coupled-channel model and the statistical model are used to analyze the measured evaporation-residue cross sections of 48 fusion reactions. The experimental data of these reactions are systematically well reproduced (within one order of magnitude). It is found that the ratio of a_f (level density parameter in fission channel) to a_n (level density parameter in neutron-evaporation channel) plays an important role in reproducing the data appropriately. Furthermore, a good exponential holds between the ratio a_f/a_n and the fissility parameter.

I. INTRODUCTION

In recent decades, the synthesis of superheavy elements and nuclei is at the frontier of research in nuclear physics [1]. In 2016, four new synthetic elements with $Z = 113$ (nihonium), 115 (moscovium), 117 (tennessine), and 118 (oganesson) have been added to the periodic table [2]. Up to now, superheavy nuclei (SHN) with $Z \leqslant 118$ have been produced via cold-fusion reactions with Pb and Bi as targets [1,3] or hot-fusion reactions with ^{48}Ca as projectiles [4,5]. The evaporation-residue (ER) cross sections σ_{ER} of the produced SHN are tiny, which makes the experiment much more difficult. In addition, the σ_{ER} of the SHN produced via fusion reactions depends strongly on the projectile-target combination and the incident energy. Hence, the theoretical study of such dependencies is useful particularly for guiding future experimental searches. For example, many efforts have been devoted to predict the optimal incident energy and the maximal σ_{ER} of the elements 119 and 120 [6–14].

Usually, the reaction process leading to the synthesis of SHN is divided into three reaction stages, namely the capture process of the colliding system to overcome the Coulomb barrier, the formation of the compound nucleus (CN) to pass over the inner fusion barrier, and the de-excitation of the excited CN against fission. Hence, the σ_{ER} can be calculated as the summation over all partial waves J [15–18]:

$$\sigma_{ER}(E_{c.m.}) = \sum_J \sigma_{capture}(E_{c.m.}, J) P_{CN}(E_{c.m.}, J) W_{sur}(E_{c.m.}, J),$$
(1)

where $\sigma_{capture}$ is the capture cross section, P_{CN} is the formation probability of a CN after the capture, and W_{sur} is the survival probability of the excited CN. $E_{c.m.}$ is the incident energy in the center-of-mass frame.

Most theoretical approaches for the formation of SHN have a similar viewpoint in the description of the capture and the

deexcitation stages [9–12,16,19–25]. A number of theoretical calculations on ER cross sections for SHN synthesis show remarkable agreement with the measured ER cross sections, while, if focusing on the theoretical values of the P_{CN}, one can find that the calculated values can differ by two or three orders of magnitude [26–28]. The large uncertainty in the calculated P_{CN} is not a surprise because of some serious ambiguities in the reaction mechanism of fusion dynamics [28]. Furthermore, it means that the calculated $\sigma_{capture}$ and W_{sur} accommodate the large discrepancies between the calculated P_{CN} from different models. In this sense, the predictive power of these models remains quite limited in giving the maximal σ_{ER} for SHN synthesis. Therefore, it is very important to examine carefully these three stages in the study of the synthesis mechanism of SHN.

For the capture process, based on a large number of capture excitation functions, recently we have developed an empirical coupled-channel (ECC) model and performed a systematic study for calculating the capture cross sections [29]. For the 220 reaction systems, the capture cross sections at energies near the Coulomb barrier are reproduced well by this ECC model [29]. In this ECC model, the effects of couplings to inelastic excitations and neutron transfer channels are effectively taken into account by introducing an empirical barrier weight function [29–31]. In addition, for the reactions with quasifission barrier high enough, that is $P_{CN} \approx 1$ [32], then the σ_{ER} can be given as

$$\sigma_{ER}(E_{c.m.}) = \sum_J \sigma_{capture}(E_{c.m.}, J) W_{sur}(E_{c.m.}, J).$$
(2)

In this case, based on the present ECC model, the measured ER cross sections can be used to constrain the key parameters in the calculations of W_{sur}. In the present work, the ECC model is adopted to calculate $\sigma_{capture}$ and the statistical model [33,34] is used to calculate W_{sur}. To refine the key parameters of the statistical model, the evaporation-residue cross sections of a series of fusion-fission reactions will be investigated.

The paper is organized as follows. In Sec. II, we introduce the ECC model and the statistical model used to calculate W_{sur}.

*bingwang@zzu.edu.cn

In Sec. III, the influence of some key parameters is studied, then the calculated σ_{ER} of a series of fusion-fission reactions compared with the data are given. Finally, a summary is given in Sec. IV.

II. CAPTURE CROSS SECTION AND SURVIVAL PROBABILITY

A. Capture cross section and the ECC model

The capture cross section at a given center-of-mass energy $E_{\text{c.m.}}$ can be written as the sum of the cross sections for each partial wave J,

$$\sigma_{\text{capture}}(E_{\text{c.m.}}) = \pi \lambdabar^2 \sum_{J}^{J_{\text{max}}} (2J + 1) T(E_{\text{c.m.}}, J). \quad (3)$$

Here $\lambdabar^2 = \hbar^2/(2\mu E_{\text{c.m.}})$ denotes the reduced de Broglie wavelength. μ is the reduced mass of the reaction system. T denotes the penetration probability of the potential barrier between the colliding nuclei at a given J. J_{max} is the critical angular momentum: For a partial wave with angular momentum larger than J_{max}, the "pocket" of the interaction potential disappears.

The penetration probability T in Eq. (3) is calculated with the ECC model in which the coupled-channel effects are taken into account by introducing a barrier distribution function $f(B)$ [29]. When the interaction potential near the Coulomb barrier is approximated by an "inverted" parabola, T can be calculated by the well-known Hill-Wheeler formula [35]. Then the penetration probability T in Eq. (3) is given as [29–31]

$$T(E_{\text{c.m.}}, J) = \int f(B) T_{\text{HW}}(E_{\text{c.m.}}, J, B) dB, \quad (4)$$

where B is the barrier height. T_{HW} is written as

$$T_{\text{HW}}(E_{\text{c.m.}}, J)$$
$$= \left\{ 1 + \exp\left[\frac{2\pi}{\hbar\omega(J)} \left(\frac{\hbar^2 J(J+1)}{2\mu R_{\text{B}}^2(J)} + B - E_{\text{c.m.}} \right) \right] \right\}^{-1}, \quad (5)$$

where $R_{\text{B}}(J)$ and $\hbar\omega(J)$ are the position of the barrier and the curvature for the Jth partial wave, respectively. $\hbar\omega(J)$ is calculated as

$$\hbar\omega(J) = \sqrt{ \left. -\frac{\hbar^2}{\mu} \frac{\partial^2}{\partial R^2} V(R, J) \right|_{R=R_{\text{B}}(J)} }. \quad (6)$$

Note that for light systems at sub-barrier energies and heavy systems at deep sub-barrier energies, the parabolic approximation is not appropriate due to the omitting of the long tail of the Coulomb potential [36]. Therefore, in these cases, the Hill-Wheeler formula does not describe properly the behavior of capture cross sections. In the present work, we are dealing with energies near and above the barrier, an energy region where the Hill-Wheeler formula can be applied.

In the present ECC model, the barrier distribution function $f(B)$ is taken to be an asymmetric Gaussian function

$$f(B) = \begin{cases} \frac{1}{N} \exp\left[-\left(\frac{B - B_{\text{m}}}{\Delta_1} \right)^2 \right], & B < B_{\text{m}}, \\ \frac{1}{N} \exp\left[-\left(\frac{B - B_{\text{m}}}{\Delta_2} \right)^2 \right], & B > B_{\text{m}}. \end{cases} \quad (7)$$

$f(B)$ satisfies the normalization condition $\int f(B) dB = 1$. $N = \sqrt{\pi}(\Delta_1 + \Delta_2)/2$ is a normalization coefficient. Δ_1, Δ_2, and B_{m} denote the left width, the right width, and the most probable value of the barrier distribution, respectively. The barrier distribution is related to the couplings to low-lying collective vibrational states, rotational states, and positive Q-value neutron transfer channels. Empirical formulas for calculating the parameters of the barrier distribution function were proposed [29]. In addition, this ECC model was extended to describe the complete fusion cross sections for the reactions involving weakly bound nuclei at above-barrier energies [37,38]. More details for the present ECC model can be found in Refs. [29,38].

B. Survival probability of a compound nucleus

An excited CN can decay via emitting photon(s), neutron(s), proton(s), or light-charged particle(s) like α particle, or via fission. The survival probability under the evaporation of a certain sequence ν of x particles is calculated as follows [39]:

$$W_{\text{sur}}(E_{\text{CN}}^*, x, J) = P_\nu(E_{\text{CN}}^*, x) \prod_{i_\nu=1}^{x} \frac{\Gamma_{i_\nu}(E_i^*, J)}{\Gamma_{\text{t}}(E_i^*, J)}, \quad (8)$$

where i_ν is the index of the evaporation step, P_ν is the probability of realization of the channel ν at the initial excitation energy E_{CN}^* of the CN. E_i^* the excitation energy before evaporating the ith particle. The total width Γ_{t} for a CN decay is the sum of partial widths of particle evaporation Γ_{i_ν}, γ emission Γ_γ, and fission Γ_{f}.

The width of particle evaporation of channel ν is given as [40]

$$\Gamma_\nu(E_i^*, J) = \frac{(2S_\nu + 1)\mu_\nu}{\pi^2 \hbar^2 \rho(E_i^*, J)}$$
$$\times \int_0^{E_i^* - B_\nu} \varepsilon \rho_d(E_i^* - B_\nu - \varepsilon, J) \sigma_{\text{inv}} d\varepsilon. \quad (9)$$

Here ρ is the level density of the decaying nucleus and ρ_d denotes the level density of the residue nucleus after the emission of the particle. S_ν and ε denote the intrinsic spin of the emitted particle and its kinetic energy, respectively. B_ν denotes the binding energy of the emitted particle with the residue nucleus. μ_ν is the reduced mass between the emitted particle and residue nucleus. σ_{inv} is the cross section for the formation of the decaying nucleus in the inverse process.

In the present work, we focus on the survival probabilities of neutron emission channels. The γ-emission channel only competes with other processes when excitation energy is smaller than the neutron binding energy and therefore is disregarded [33,42]. Furthermore, for light-charged-particle emission channels, we only consider the proton and α particle
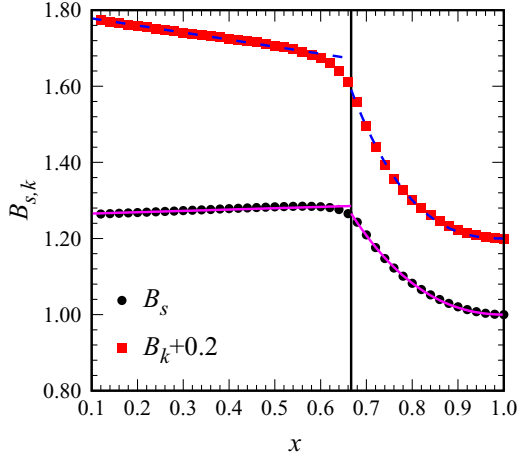
FIG. 1. The values of B_s (black dots) and B_k (red squares) as a function of the fissility parameter x taken from [41]. The solid line and the dashed line denote the results of formula (16) and formula (17), respectively.

emissions. For the evaporation of x ($x > 1$) neutron channels, the probability of realization is given by the formula proposed by Jackson [43],

$$P(E_{\mathrm{CN}}^*, x) = I(\Delta_x, 2x - 3) - I(\Delta_{x+1}, 2x - 1). \qquad (10)$$

Here, $I(z, m) = \frac{1}{m!} \int_0^z u^m e^{-u} du$ is Pearson's incomplete gamma function. $\Delta_x = [E_{\mathrm{CN}}^* - \sum_{i=1}^{x} B_{\mathrm{n}}(i)]/T$, $B_{\mathrm{n}}(i)$ is the separation energy of the ith evaporated neutron. In the present work, B_{n} is calculated by the Weizsäcker-Skyrme (WS) mass formula [44,45].

The fission width can be calculated with the Bohr-Wheeler formula [46] as

$$\Gamma_{\mathrm{f}}(E_i^*, J) = \frac{1}{2\pi \rho(E_i^*, J)} \int_{-B_{\mathrm{f}}}^{E_i^* - B_{\mathrm{f}}} \frac{\rho_{\mathrm{sd}}(E_i^* - B_{\mathrm{f}} - \varepsilon, J)}{1 + \exp[-2\pi\varepsilon/\hbar\omega]} d\varepsilon, \qquad (11)$$

where ρ_{sd} is the level density at the saddle point. $\hbar\omega$ denotes the curvature of the fission barrier and is taken to be 2.2 MeV. The fission barrier B_{f} consists of a macroscopic liquid-drop component and a microscopic shell correction energy including the washing out effect, which is written as [39,47]

$$B_{\mathrm{f}} = B_{\mathrm{f}}^{\mathrm{mac}} + B_{\mathrm{f}}^{\mathrm{mic}} \exp(-E^*/E_d), \qquad (12)$$

with E_d being the shell damping energy and taken to be 18.5 MeV [48]. The macroscopic liquid-drop component $B_{\mathrm{f}}^{\mathrm{mac}}$ is given by [41,49]

$$B_{\mathrm{f}}^{\mathrm{mac}} = \begin{cases} 0.38(3/4 - x)E_{\mathrm{s0}}, & 1/3 < x < 2/3, \\ 0.83(1 - x)^3 E_{\mathrm{s0}}, & 2/3 < x < 1, \end{cases} \qquad (13)$$

where $E_{\mathrm{s0}} = 17.944[1 - 1.7826[(N - Z)/A]^2]A^{2/3}$ denotes the surface energy for the equivalent spherical nucleus and $E_{\mathrm{c0}} = 0.7053Z^2/A^{1/3}$ is the Coulomb energy for the equivalent spherical nucleus. $x = E_{\mathrm{c0}}/2E_{\mathrm{s0}}$ is the fissility parameter. The shell correction energy $B_{\mathrm{f}}^{\mathrm{mic}}$ is calculated by the WS mass formula [44,45].
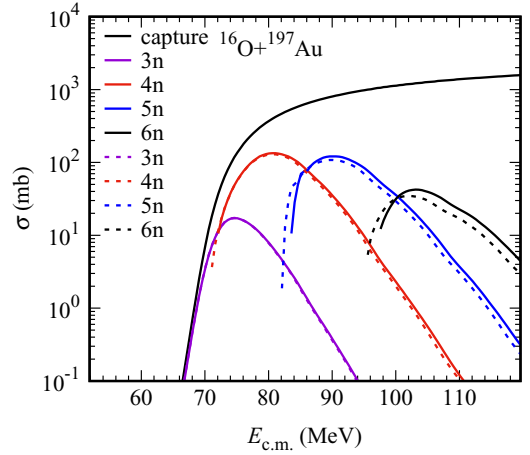

FIG. 2. The capture and ER cross sections of reaction $^{16}\mathrm{O} + ^{197}\mathrm{Au}$. The solid lines denote the ER cross sections calculated with $r_0 = 1.1$. The dotted lines show the ER cross sections calculated with $r_0 = 1.2$.

The level density is calculated with the Fermi-gas model [47] as

$$\rho(E^*, J) = \frac{2J + 1}{24\sqrt{2}\sigma^3 a^{1/4}(E^* - \delta)^{5/4}}$$
$$\times \exp\left[2\sqrt{a(E^* - \delta)} - \frac{(J + 1/2)^2}{2\sigma^2}\right], \qquad (14)$$

where $\sigma^2 = 6\bar{m}^2\sqrt{a(E^* - \delta)}/\pi^2$ and the average projection of the angular momentum of single-particle states at Fermi surface $\bar{m}^2 \approx 0.24A^{2/3}$. The pairing correction δ is set to be $-12/\sqrt{A}$ MeV, 0, and $12/\sqrt{A}$ MeV for odd-odd, even-odd, and even-even nuclei, respectively.
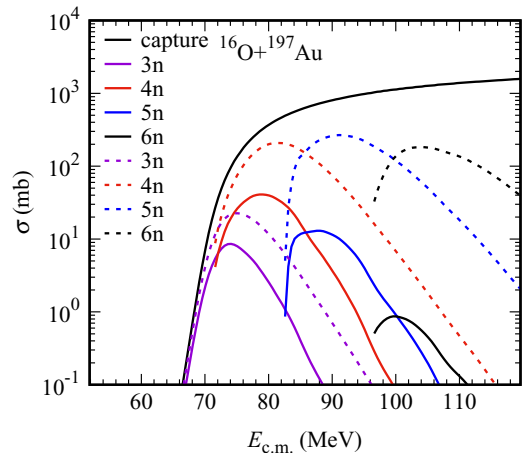

FIG. 3. The capture and ER cross sections of reaction $^{16}\mathrm{O} + ^{197}\mathrm{Au}$. The solid lines denote the ER cross sections calculated with $a_{\mathrm{f}}/a_{\mathrm{n}} = 1.1$. The dotted lines show the ER cross sections calculated with $a_{\mathrm{f}}/a_{\mathrm{n}} = 1.01$.
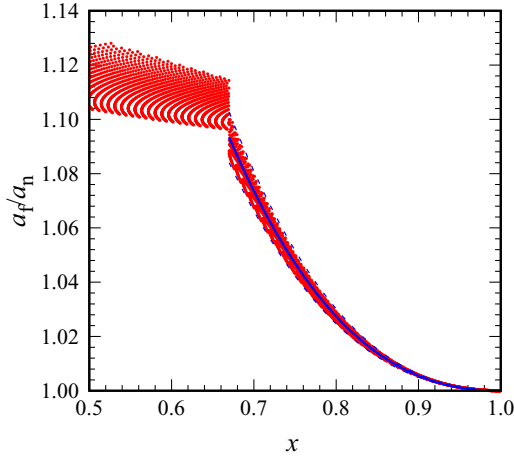
FIG. 4. The ratio of a_f to a_n as a function of the fissility parameter x. The solid line denotes the results of the formula $f(x) = a_f/a_n = 1.319(1-x)^3 + 0.422(1-x)^2 + 1$ and the dashed lines show the boundaries of 10% uncertainty of $f(x)$.

III. RESULTS AND DISCUSSIONS

We first investigate the key parameters of the statistical model for calculating the survival probability. Then for 48 reactions with $P_{CN} \approx 1$, i.e., quasifission barrier high enough, we will show the comparison of the calculated evaporation-residue cross section with the experimental values.

A. Level density parameters

In the calculations of the survival probability, the level density parameter a is one of the key parameters. Usually, the level density parameter is taken to be dependent on the nuclear

mass number from $A/12$ to $A/8$. In the present work, the level density parameter a taking into account the volume, surface, and curvature dependence of the single-particle level density at the Fermi surface is adopted and given by [48]

$$a = 0.04543 r_0^3 A + 0.1355 r_0^2 A^{2/3} B_s + 0.1426 r_0 A^{1/3} B_k, \quad (15)$$

with B_s and B_k being the surface and curvature factors defined in the droplet model. r_0 is the radius parameter, which is set to 1.16 fm in the following calculations. For example, for a spherical nucleus ($B_s = B_k = 1$) with $A = 100$ one gets $a = 11.786 \approx A/8.5$, while for $A = 200$ one gets $a = 21.385 \approx A/9.4$. For evaporation channels, B_s and B_k are taken to be 1. For the level density parameter of fission channel a_f, the formula (15) is in a form that is very suitable for calculating the fission probability, since it contains with B_s and B_k a shape dependence in a form reminiscent of droplet model formulas [48]. a_f/a_n (a_n level density parameter for the neutron-evaporation channel) becomes systematically larger than 1 because of the surface being systematically larger at the saddle point.

The values of B_s and B_k were tabulated as a function of the fissility parameter x [41], which is shown in Fig. 1. It can be seen that B_s and B_k have a linear relation with x in the region of $x < 2/3$ and an exponential relation with x in the region of $x > 2/3$. Therefore, by fitting the values, formulas for calculating B_s and B_k can be obtained as

$$B_s = \begin{cases} -0.035(1-x) + 1.297, & x < 2/3, \\ 2.409(1-x)^3 + 1.587(1-x)^2 + 1, & 2/3 < x < 1 \end{cases} \quad (16)$$
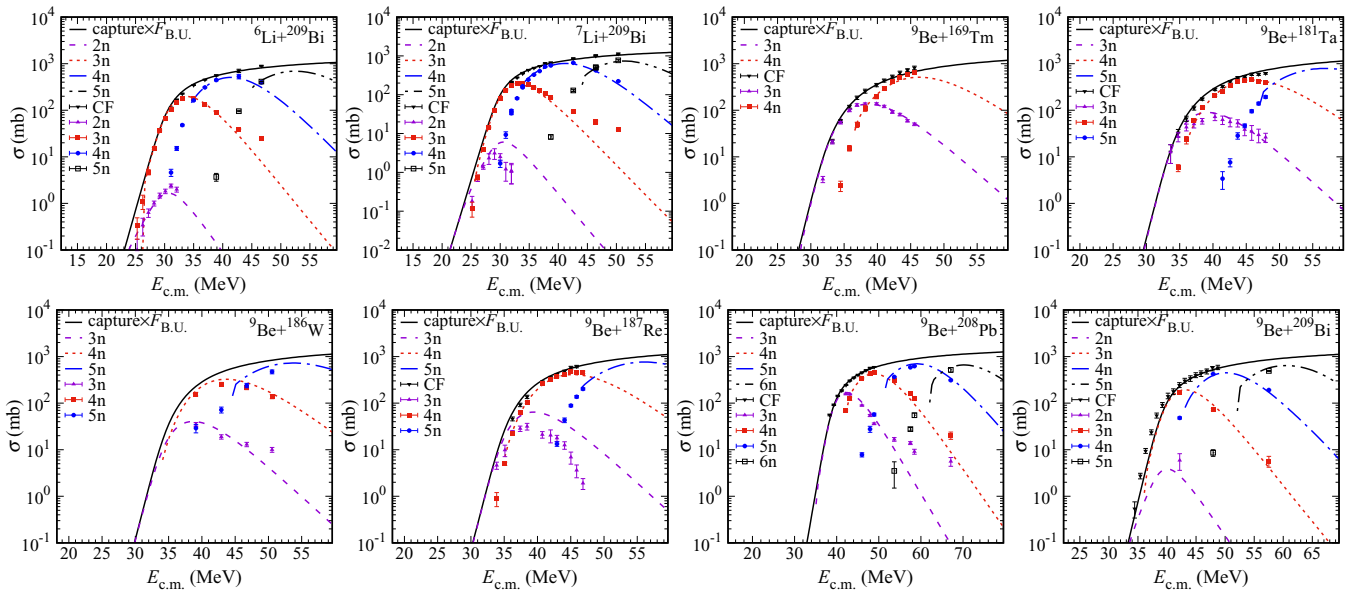

FIG. 5. The cross sections of reactions $^{6,7}\text{Li} + ^{209}\text{Bi}$ [50], $^9\text{Be} + ^{169}\text{Tm}$ [51], $^9\text{Be} + ^{181}\text{Ta}$ [52], $^9\text{Be} + ^{186}\text{W}$ [52], $^9\text{Be} + ^{187}\text{Re}$ [51], $^9\text{Be} + ^{208}\text{Pb}$ [50], and $^9\text{Be} + ^{209}\text{Bi}$ [53,54]. The black solid line denotes $\sigma_{capture}$ scaled by the suppression factor, i.e., $F_{B.U.}$ taken from Ref. [37]. CF denotes the data of the complete fusion cross sections. The calculated results and the data of the σ_{ER} for neutron-evaporation channels are shown by the various dotted lines and symbols (denoted with xn).
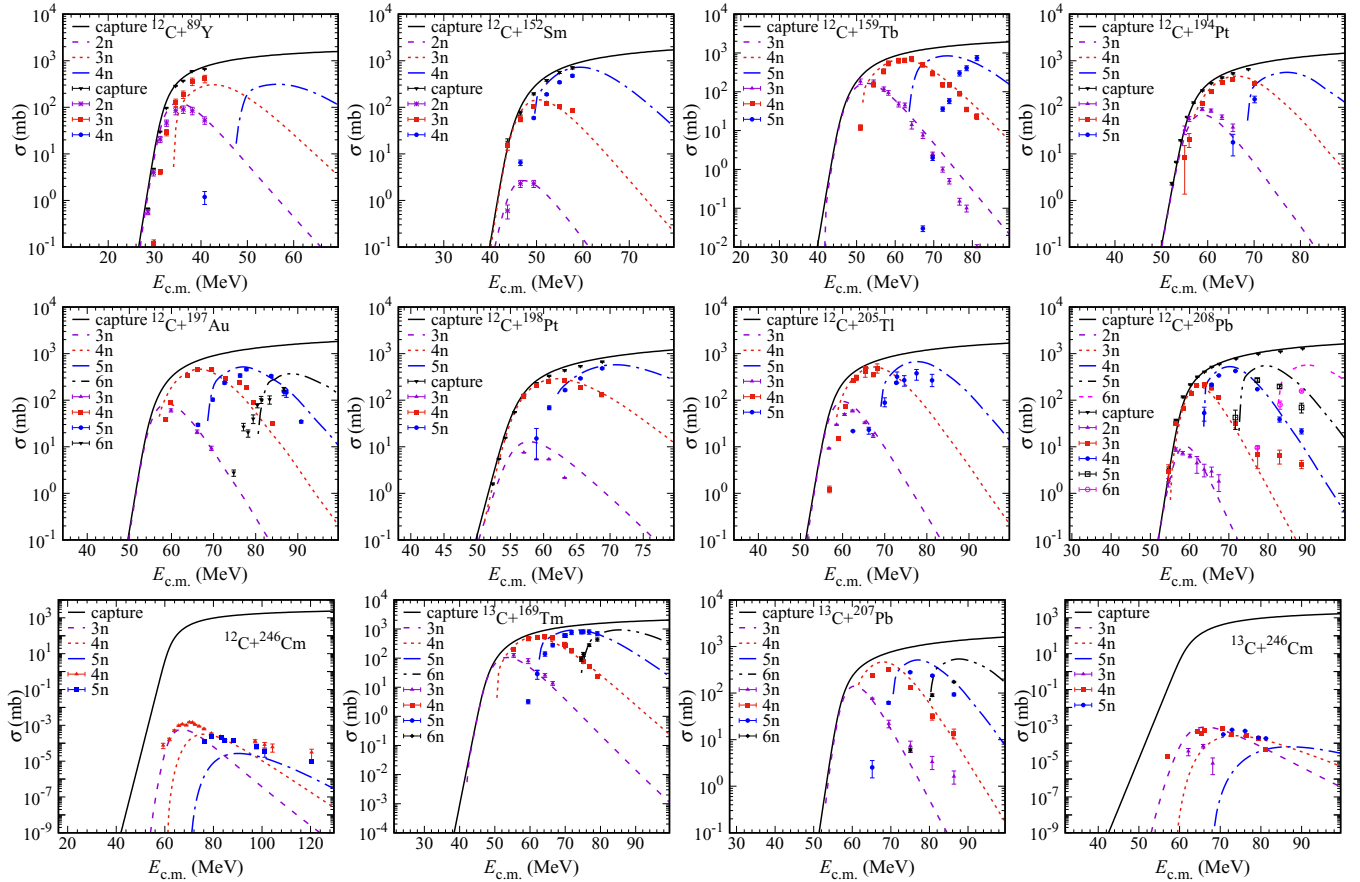
FIG. 6. The cross sections for reactions induced by ^{12}C on ^{89}Y [55], ^{152}Sm [56], ^{159}Tb [57], ^{194,198}Pt [58], ^{197}Au [59], ^{205}Tl [60], ^{208}Pb [61], and ^{246}Cm [62] and ^{13}C on ^{169}Tm [63], ^{207}Pb [61], and ^{246}Cm [62]. The black solid line denotes σ_{capture}. The calculated results and the data of the σ_{ER} for neutron-evaporation channels are shown by the various dotted lines and symbols (denoted with xn).

and

$$B_k = \begin{cases} 0.186(1-x) + 1.411, & x < 2/3, \\ 7.461(1-x)^3 + 1.028(1-x)^2 + 1, & 2/3 < x < 1 \end{cases} \tag{17}$$

respectively. Therefore, in the present work, for the fission channel, a_f is calculated by the formulas (15)–(17).

It is interesting to note that, while the absolute values of a are sensitive to r_0, the ratio a_f/a_n is insensitive to r_0. For example, if one changes r_0 from 1.16 to 1.20, the value for the ratio a_f/a_n in ^{208}Pb changes from 1.079 to 1.082. Taking the reaction ^{16}O + ^{197}Au as an example, the sensitivity of r_0 to the calculated ER cross sections of neutron-evaporation channels is investigated and shown in Fig. 2. The solid lines and the dotted lines show the ER cross sections calculated with $r_0 = 1.1$ and $r_0 = 1.2$, respectively. One can find that the calculated ER cross sections are insensitive to r_0. In addition, the sensitivity of the ratio a_f/a_n to the calculated ER cross sections is also investigated and shown in Fig. 3. The solid lines and the dotted lines show the ER cross sections calculated with $a_f/a_n = 1.1$ and $a_f/a_n = 1.01$, respectively. It can be seen that the calculated ER cross sections are much smaller with the larger ratio, i.e., $a_f/a_n = 1.1$ because of

the ratio Γ_n/Γ_f being smaller. Furthermore, with the larger ratio a_f/a_n, the washing out effect of the shell correction energy on the ER cross sections becomes stronger, which is means that the ER cross sections decrease faster with the increase of energy. Therefore, the calculated ER cross sections of neutron-evaporation channels are sensitive to the ratio a_f/a_n since W_{sur} of the neutron-evaporation channels is mainly determined by the ratio Γ_n/Γ_f. Therefore, to reproduce the trend of the data for ER cross sections of neutron-evaporation channels, the ratio a_f/a_n plays the key rule, in particular, for the cases in which fission dominates the decay of a CN.

Usually, a_f/a_n is empirically taken to be 1.1 in the calculations of the survival probability. For nuclei with $x > 0.5$, the calculated values of a_f/a_n with formulas (15)–(17) are shown in Fig. 4. It can be seen that $a_f/a_n = 1.1$ is a good approximation for nuclei with $x < 2/3$. In the region of $2/3 < x < 1$, a_f/a_n decreases exponentially with increasing x. In this case, a_f/a_n can be calculated approximately by the formula of $f(x) = a_f/a_n = 1.319(1-x)^3 + 0.422(1-x)^2 + 1$ of which the uncertainty is 10%. $f(x)$ is obtained by fitting the calculated values of a_f/a_n. The solid line in Fig. 4 denotes the results of $f(x)$ and the dashed lines show the boundaries of 10% percent uncertainty of $f(x)$.
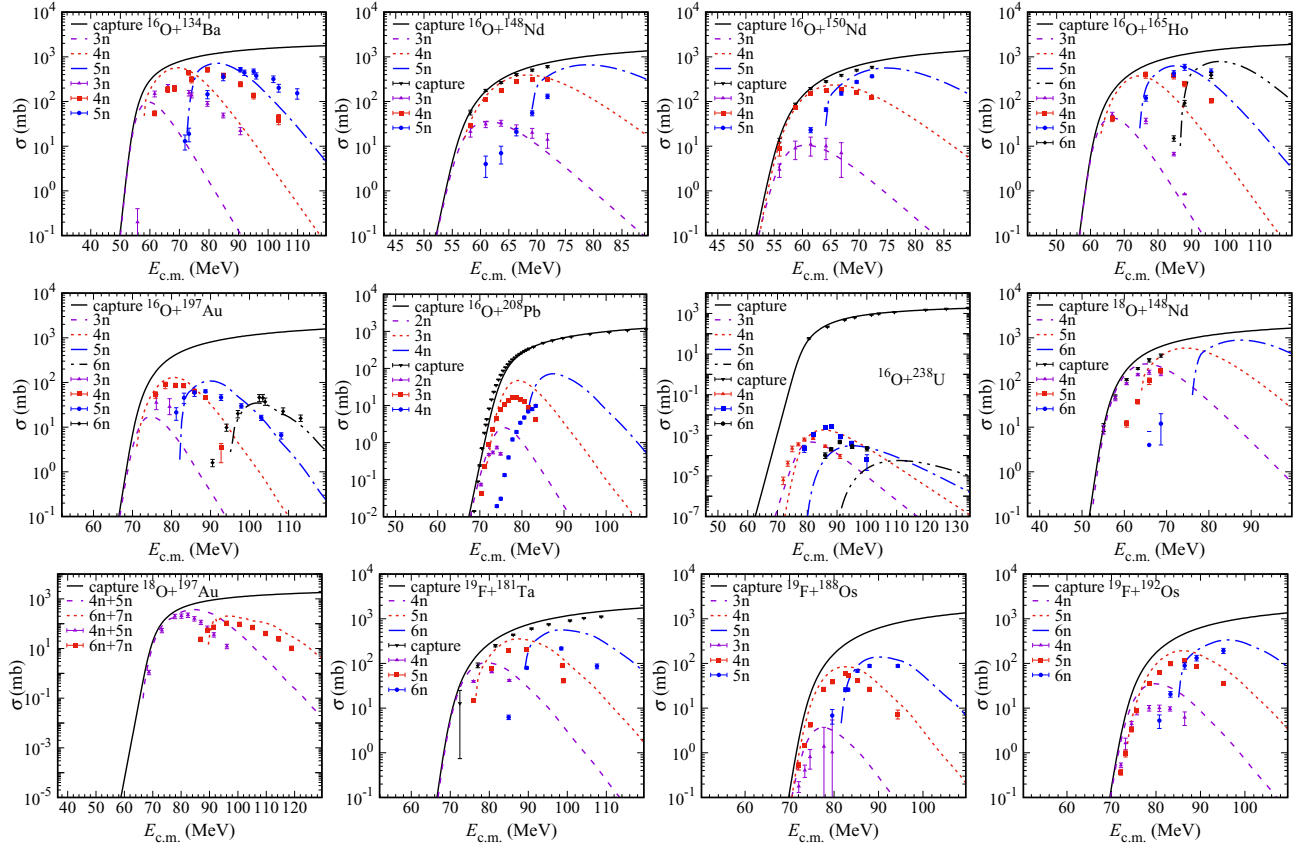
FIG. 7. The cross sections for reactions induced by ^{16}O on ^{134}Ba [64], ^{148,150}Nd [56], ^{165}Ho [65], ^{197}Au [66], ^{208}Pb [67], and ^{238}U [68], ^{18}O on ^{148}Nd [56] and ^{197}Au [69], and ^{19}F on ^{181}Ta [70] and ^{188,192}Os [71]. The black solid line denotes σ_{capture}. The calculated results and the data of the σ_{ER} for neutron-evaporation channels are shown by the various dotted lines and symbols (denoted with xn).

B. Comparison between the calculated ER cross sections and the data

Based on the discussions on the key parameters in the calculations of the survival probability, 48 reactions with $P_{\text{CN}} \approx 1$, i.e., quasi-fission barrier high enough, are investigated. The fission barrier of the CN is calculated by Eqs. (12) and (13); the correction energy $B_{\text{f}}^{\text{mic}}$ and the neutron-separation energy B_{n} are calculated by the WS mass formula [44,45]. Therefore, there are no free parameters in the following calculations of the ER cross sections.

Figure 5 shows the comparison of the calculated complete fusion cross sections and σ_{ER} with the experimental values for the reactions involving weakly bound nuclei ^{6,7}Li and ^{9}Be. For these reactions, owing to the breakup of the weakly bound projectiles, the complete fusion (CF) cross sections are suppressed at energies above the Coulomb barrier. The systematics of the suppression effects on CF in these reactions have been obtained [37,38]. It is found that the suppression of CF cross sections are roughly independent of the target for the reactions induced by the same projectile. Furthermore, the suppression factors $F_{\text{B.U.}}$ for ^{6,7}Li and ^{9}Be induced reactions are 0.6, 0.67, and 0.68, respectively [37]. Then the calculated complete fusion cross sections, i.e., σ_{capture} scaled by $F_{\text{B.U.}}$ are shown by the black solid line. The data of the complete fusion cross sections are denoted with CF in Fig. 5. It can be

seen that the CF cross sections of the reactions are reproduced well. Moreover, the ER cross sections of neutron-evaporation channels are calculated and shown by the various dotted lines (denoted with xn). The experimental data are also presented for comparison. It can be seen that the data of the σ_{ER} are also reproduced well.

TABLE I. The fissility parameter and the calculated $a_{\text{f}}/a_{\text{n}}$ of the CN produced by the reactions.

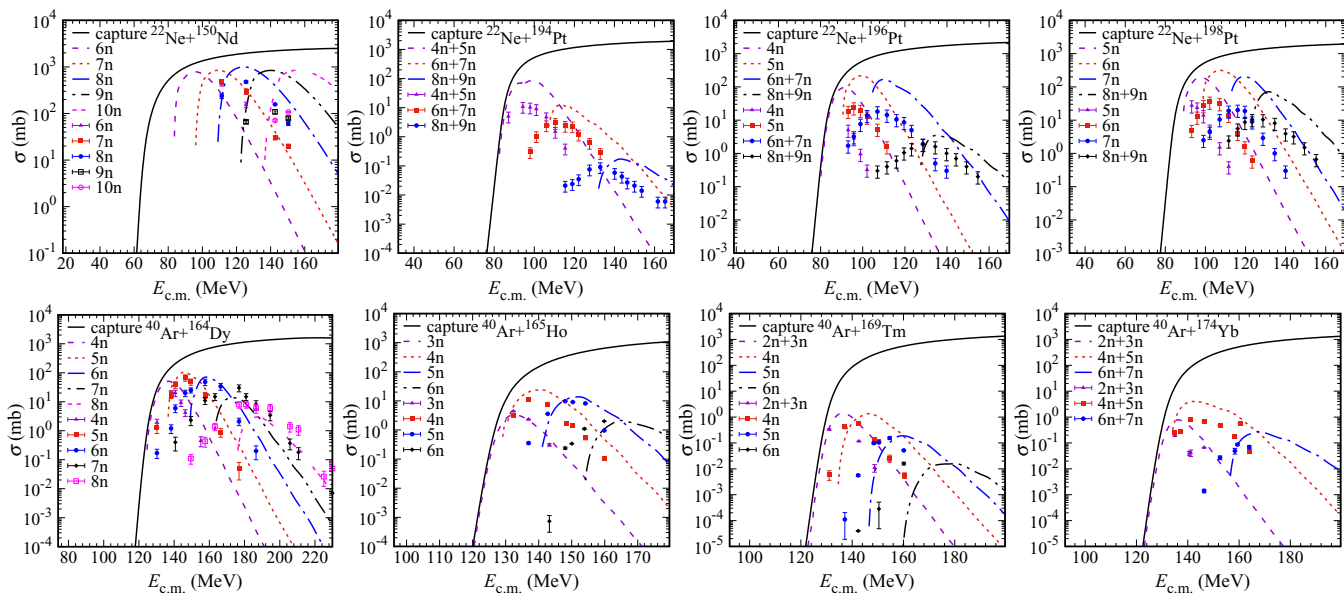| Reactions	CN	x	$a_{\text{f}}/a_{\text{n}}$
^{12}C + ^{246}Cm	^{258}No	0.860	1.012
^{13}C + ^{246}Cm	^{259}No	0.858	1.012
^{16}O + ^{197}Au	^{213}Fr	0.743	1.051
^{18}O + ^{197}Au	^{215}Fr	0.740	1.052
^{16}O + ^{238}U	^{254}Fm	0.842	1.016
^{22}Ne + ^{150}Nd	^{172}Yb	0.597	1.109
^{22}Ne + ^{194}Pt	^{216}Ra	0.750	1.047
^{22}Ne + ^{196}Pt	^{218}Ra	0.748	1.048
^{22}Ne + ^{198}Pt	^{220}Ra	0.745	1.049
^{40}Ar + ^{164}Dy	^{204}Po	0.720	1.063
^{40}Ar + ^{165}Ho	^{205}At	0.731	1.057
^{40}Ar + ^{169}Tm	^{209}Fr	0.749	1.048
^{40}Ar + ^{174}Yb	^{214}Ra	0.753	1.046

FIG. 8. The capture cross section and the evaporation-residue cross section of (xn) channels for reactions induced by ^{22}Ne on ^{150}Nd [72] and ^{194,196,198}Pt [73] and ^{40}Ar on ^{164}Dy [74], ^{165}Ho [75], ^{169}Tm [75], and ^{174}Yb [75]. The black solid line denotes σ_{capture}. The calculated results and the data of the σ_{ER} for neutron-evaporation channels are shown by the various dotted lines and symbols (denoted with xn).

In Figs. 6–9, we present the comparison of the calculated σ_{capture} and σ_{ER} with the experimental values for the reactions induced by ^{12,13}C, ^{16,18}O, ^{19}F, ^{22}Ne, ^{28,30}Si, ^{31}P, ^{34}S, ^{40}Ar, and ^{48}Ti, and ^{58,64}Ni. The solid black line denotes the calculated capture cross sections. The ER cross sections of neutron-evaporation channels are calculated and shown by the various dotted lines (denoted with xn). Furthermore the experimental data are also presented for comparison. It can be seen that the experimental data for these reactions are systematically well

reproduced (within one order of magnitude) at energies near and above the Coulomb barrier.

As mentioned above, the ratio $a_{\text{f}}/a_{\text{n}}$ plays the key rule in reproducing the data, in particular for the cases in which fission dominates the decay of a CN. Therefore, here one can focus on the reactions in which the dominant decay mode of the CN is fission, such as ^{12,13}C + ^{246}Cm, ^{16,18}O + ^{197}Au, ^{16}O + ^{238}U, and the reactions induced by ^{22}Ne and ^{40}Ar. The fissility parameter and the calculated $a_{\text{f}}/a_{\text{n}}$ of the CN
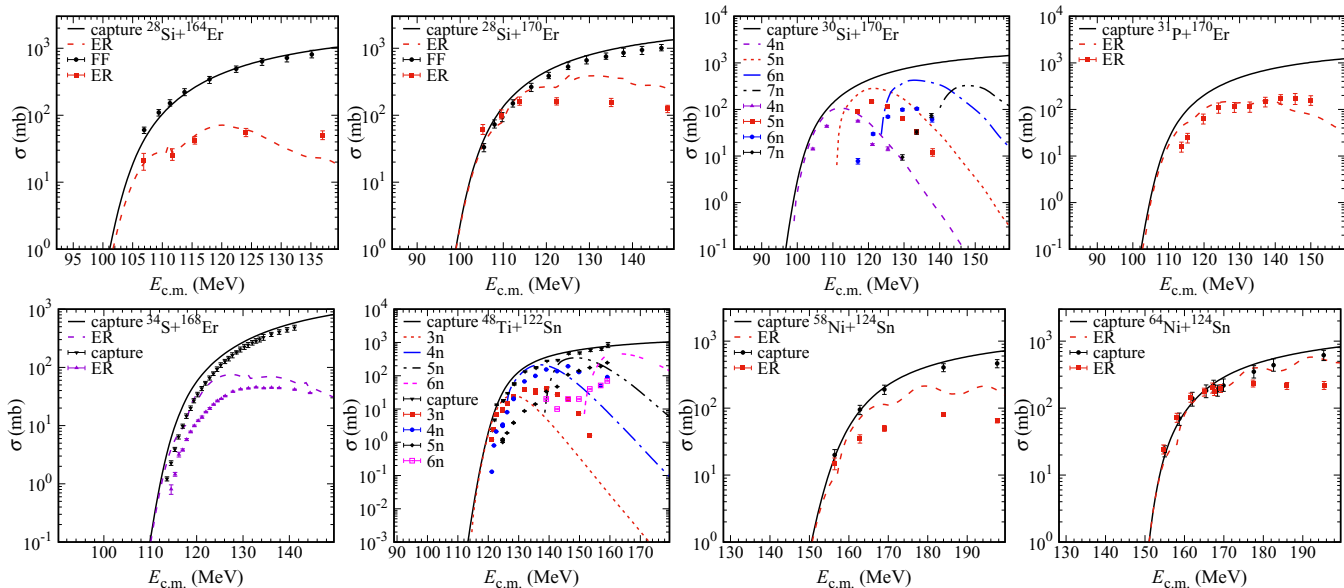

FIG. 9. The capture cross section and the evaporation-residue cross sections for reactions ^{28}Si + ^{164,170}Er [76,77], ^{30}Si + ^{170}Er [70], ^{31}P + ^{170}Er [78], ^{34}S + ^{168}Er [79], ^{48}Ti + ^{122}Sn [80], and ^{58,64}Ni + ^{124}Sn [76,81], The black solid line denotes σ_{capture}. The calculated results and the data of the σ_{ER} for neutron-evaporation channels are shown by the various dotted lines and symbols (denoted with xn).

produced in these reactions are tabulated in Table I. For these reactions, one can find that the trend of the ER cross sections of neutron-evaporation channels is well reproduced. One can conclude that the values of a_f/a_n adopted in the calculations are reasonable. Hence the survival probabilities of a CN calculated with the level density parameter given by formula (15) are reliable.

IV. SUMMARY

The empirical coupled-channel model and the statistical model are used to analyze the measured evaporation-residue cross sections of fusion-fission reactions. To reduce the uncertainty of the prediction of the survival probability of a compound nucleus, the level density parameter in the statistical model has been investigated by performing a sys-

tematically study of the evaporation-residue cross sections for 48 reactions. It is found that the ratio of a_f (level density parameter in fission channel) to a_n (level density parameter in neutron-evaporation channel) plays an important role in reproducing the data appropriately. Furthermore, a good exponential relation holds between the ratio a_f/a_n and the fissility parameter. With the investigation of capture cross sections and the survival probabilities of the compound nuclei, the ambiguity of the prediction of fusion probabilities could be reduced. Work on these aspects is in progress.

[1] S. Hofmann and G. Münzenberg, Rev. Mod. Phys. **72**, 733 (2000).

[2] W. Nazarewicz, Nat. Phys. **14**, 537 (2018).

[3] K. Morita, K. Morimoto, D. Kaji, T. Akiyama, S. ichi Goto, H. Haba, E. Ideguchi, R. Kanungo, K. Katori, H. Koura, H. Kudo, T. Ohnishi, A. Ozawa, T. Suda, K. Sueki, H. Xu, T. Yamaguchi, A. Yoneda, A. Yoshida, and Y. Zhao, J. Phys. Soc. Jpn. **73**, 2593 (2004).

[4] Y. Oganessian, J. Phys. G: Nucl. Part. Phys. **34**, R165 (2007).

[5] Y. T. Oganessian, F. S. Abdullin, P. D. Bailey, D. E. Benker, M. E. Bennett, S. N. Dmitriev, J. G. Ezold, J. H. Hamilton, R. A. Henderson, M. G. Itkis, Y. V. Lobanov, A. N. Mezentsev, K. J. Moody, S. L. Nelson, A. N. Polyakov, C. E. Porter, A. V. Ramayya, F. D. Riley, J. B. Roberto, M. A. Ryabinin *et al.*, Phys. Rev. Lett. **104**, 142502 (2010).

[6] V. Zagrebaev and W. Greiner, Phys. Rev. C **78**, 034610 (2008).

[7] N. Wang, J. Tian, and W. Scheid, Phys. Rev. C **84**, 061601(R) (2011).

[8] Z.-H. Liu and J.-D. Bao, Phys. Rev. C **84**, 031602(R) (2011).

[9] N. Wang, E.-G. Zhao, W. Scheid, and S.-G. Zhou, Phys. Rev. C **85**, 041601(R) (2012).

[10] J. Zhang, C. Wang, and Z. Ren, Nucl. Phys. A **909**, 36 (2013).

[11] G. G. Adamian, N. V. Antonenko, and W. Scheid, Eur. Phys. J. A **41**, 235 (2009).

[12] X. J. Bao, Y. Gao, J. Q. Li, and H. F. Zhang, Phys. Rev. C **91**, 011603(R) (2015).

[13] X. J. Bao, Y. Gao, J. Q. Li, and H. F. Zhang, Phys. Rev. C **92**, 034612 (2015).

[14] X. J. Bao, Y. Gao, J. Q. Li, and H. F. Zhang, Phys. Rev. C **92**, 014601 (2015).

[15] N. V. Antonenko, E. A. Cherepanov, A. K. Nasirov, V. P. Permjakov, and V. V. Volkov, Phys. Lett. B **319**, 425 (1993).

[16] N. V. Antonenko, E. A. Cherepanov, A. K. Nasirov, V. P. Permjakov, and V. V. Volkov, Phys. Rev. C **51**, 2635 (1995).

[17] E. A. Cherepanov, V. V. Volkov, N. V. Antonenko, V. P. Permjakov, and A. K. Nasirov, Nucl. Phys. A **583**, 165 (1995).

[18] G. G. Adamian, N. V. Antonenko, W. Scheid, and V. V. Volkov, Nucl. Phys. A **627**, 361 (1997).

[19] G. G. Adamian, N. V. Antonenko, and W. Scheid, Nucl. Phys. A **678**, 24 (2000).

[20] Z. Liu and J. Bao, Sci. China G **49**, 641 (2007).

[21] Z.-Q. Feng, G.-M. Jin, J.-Q. Li, and W. Scheid, Phys. Rev. C **76**, 044606 (2007).

[22] C. Wang, J. Zhang, Z. Z. Ren, and C. W. Shen, Phys. Rev. C **82**, 054605 (2010).

[23] L. Zhu, Z.-Q. Feng, C. Li, and F.-S. Zhang, Phys. Rev. C **90**, 014612 (2014).

[24] W. J. Świątecki, K. Siwek-Wilczyńska, and J. Wilczyński, Phys. Rev. C **71**, 014602 (2005).

[25] W. Loveland, Phys. Rev. C **76**, 014612 (2007).

[26] R. S. Naik, W. Loveland, P. H. Sprunger, A. M. Vinodkumar, D. Peterson, C. L. Jiang, S. Zhu, X. Tang, E. F. Moore, and P. Chowdhury, Phys. Rev. C **76**, 054604 (2007).

[27] L. Zhu, W.-J. Xie, and F.-S. Zhang, Phys. Rev. C **89**, 024615 (2014).

[28] H. Lü, D. Boilley, Y. Abe, and C. Shen, Phys. Rev. C **94**, 034616 (2016).

[29] B. Wang, K. Wen, W.-J. Zhao, E.-G. Zhao, and S.-G. Zhou, At. Data Nucl. Data Tables **114**, 281 (2017).

[30] B. Wang, W. Zhao, E. Zhao, and S. Zhou, Sci. China Phys. Mech. Astron. **59**, 642002 (2016).

[31] B. Wang, W.-J. Zhao, E.-G. Zhao, and S.-G. Zhou, Phys. Rev. C **98**, 014615 (2018).

[32] N. Wang, K. Zhao, W. Scheid, and X. Wu, Phys. Rev. C **77**, 014603 (2008).

[33] A. S. Zubov, G. G. Adamian, N. V. Antonenko, S. P. Ivanova, and W. Scheid, Phys. Rev. C **65**, 024308 (2002).

[34] C. Xia, B. Sun, E. Zhao, and S. Zhou, Sci. China-Phys. Mech. Astron. **54** (Suppl. 1), s109 (2011).

[35] D. L. Hill and J. A. Wheeler, Phys. Rev. **89**, 1102 (1953).

[36] L.-L. Li, S.-G. Zhou, E.-G. Zhao, and W. Scheid, Int. J. Mod. Phys. E **19**, 359 (2010).

[37] B. Wang, W.-J. Zhao, P. R. S. Gomes, E.-G. Zhao, and S.-G. Zhou, Phys. Rev. C **90**, 034612 (2014).

[38] B. Wang, W.-J. Zhao, A. Diaz-Torres, E.-G. Zhao, and S.-G. Zhou, Phys. Rev. C **93**, 014615 (2016).

[39] A. S. Zubov, G. G. Adamian, N. V. Antonenko, S. P. Ivanova, and W. Scheid, Phys. Rev. C **68**, 014616 (2003).

[40] V. Weisskopf and D. Ewing, Phys. Rev. **57**, 472 (1940).

[41] W. D. Myers and W. J. Swiatecki, Ann. Phys. (NY) **84**, 186 (1974).

[42] G. G. Adamian, N. V. Antonenko, S. P. Ivanova, and W. Scheid, Phys. Rev. C **62**, 064303 (2000).

[43] J. D. Jackson, Can. J. Phys. **34**, 767 (1956).

[44] N. Wang, M. Liu, and X. Wu, Phys. Rev. C **81**, 044322 (2010).

[45] N. Wang, Z. Liang, M. Liu, and X. Wu, Phys. Rev. C **82**, 044304 (2010).

[46] N. Bohr and J. A. Wheeler, Phys. Rev. **56**, 426 (1939).

[47] Z.-Q. Feng, G.-M. Jin, F. Fu, and J.-Q. Li, Nucl. Phys. A **771**, 50 (2006).

[48] W. Reisdorf, Z. Phys. A **300**, 227 (1981).

[49] S. Cohen and W. J. Swiatecki, Ann. Phys. (NY) **22**, 406 (1963).

[50] M. Dasgupta, P. R. S. Gomes, D. J. Hinde, S. B. Moraes, R. M. Anjos, A. C. Berriman, R. D. Butt, N. Carlin, J. Lubian, C. R. Morton, J. O. Newton, and A. Szanto de Toledo, Phys. Rev. C **70**, 024606 (2004).

[51] Y. D. Fang, P. R. S. Gomes, J. Lubian, M. L. Liu, X. H. Zhou, D. R. Mendes Junior, N. T. Zhang, Y. H. Zhang, G. S. Li, J. G. Wang, S. Guo, Y. H. Qiang, B. S. Gao, Y. Zheng, X. G. Lei, and Z. G. Wang, Phys. Rev. C **91**, 014608 (2015).

[52] N. T. Zhang, Y. D. Fang, P. R. S. Gomes, J. Lubian, M. L. Liu, X. H. Zhou, G. S. Li, J. G. Wang, S. Guo, Y. H. Qiang, Y. H. Zhang, D. R. Mendes Junior, Y. Zheng, X. G. Lei, B. S. Gao, Z. G. Wang, K. L. Wang, and X. F. He, Phys. Rev. C **90**, 024621 (2014).

[53] C. Signorini, Z. H. Liu, A. Yoshida, T. Fukuda, Z. C. Li, K. E. G. Löbner, L. Müller, Y. H. Pu, K. Rudolph, F. Soramel, C. Zotti, and J. L. Sida, Eur. Phys. J. A **2**, 227 (1998).

[54] M. Dasgupta, D. J. Hinde, S. L. Sheehy, and B. Bouriquet, Phys. Rev. C **81**, 024608 (2010).

[55] C. S. Palshetkar, S. Santra, A. Chatterjee, K. Ramachandran, S. Thakur, S. K. Pandit, K. Mahata, A. Shrivastava, V. V. Parkar, and V. Nanal, Phys. Rev. C **82**, 044608 (2010).

[56] R. Broda, M. Ishihara, B. Herskind, H. Oeschler, S. Ogaza, and H. Ryde, Nucl. Phys. A **248**, 356 (1975).

[57] A. Yadav, V. R. Sharma, P. P. Singh, D. P. Singh, M. K. Sharma, U. Gupta, R. Kumar, B. P. Singh, R. Prasad, and R. K. Bhowmik, Phys. Rev. C **85**, 034614 (2012).

[58] A. Shrivastava, S. Kailas, A. Chatterjee, A. M. Samant, A. Navin, P. Singh, and B. S. Tomar, Phys. Rev. Lett. **82**, 699 (1999).

[59] S. Baba, K. Hata, S. Ichikawa, T. Sekine, Y. Nagame, A. Yokoyama, M. Shoji, T. Saito, N. Takahashi, H. Baba, and I. Fujiwara, Z. Phys. A **331**, 53 (1988).

[60] Y. Le Beyec, M. Lefort, and M. Sarda, Nucl. Phys. A **192**, 405 (1972).

[61] K. Kalita, J. Phys. G: Nucl. Part. Phys. **38**, 095104 (2011).

[62] T. Sikkeland, A. Ghiorso, and M. J. Nurmia, Phys. Rev. **172**, 1232 (1968).

[63] V. R. Sharma, A. Yadav, P. P. Singh, D. P. Singh, S. Gupta, M. K. Sharma, I. Bala, R. Kumar, S. Murlithar, B. P. Singh, and R. Prasad, Phys. Rev. C **89**, 024608 (2014).

[64] S. Della Negra, H. Gauvin, H. Jungclas, Y. Le Beyec, and M. Lefort, Z. Phys. A **282**, 65 (1977).

[65] K. Kumar, T. Ahmad, S. Ali, I. A. Rizvi, A. Agarwal, R. Kumar, K. S. Golda, and A. K. Chaubey, Phys. Rev. C **87**, 044608 (2013).

[66] S. Baba, K. Hata, S. Ichikawa, Y. Nagame, A. Yokoyama, M. Shoji, T. Saito, N. Takahashi, H. Baba, and I. Fujiwara, Z. Phys. A **331**, 53 (1988).

[67] C. R. Morton, D. J. Hinde, J. R. Leigh, J. P. Lestone, M. Dasgupta, J. C. Mein, J. O. Newton, and H. Timmers, Phys. Rev. C **52**, 243 (1995).

[68] K. Nishio, H. Ikezoe, Y. Nagame, M. Asai, K. Tsukada, S. Mitsuoka, K. Tsuruta, K. Satou, C. J. Lin, and T. Ohsawa, Phys. Rev. Lett. **93**, 162701 (2004).

[69] L. Corradi, B. R. Behera, E. Fioretto, A. Gadea, A. Latina, A. M. Stefanini, S. Szilner, M. Trotta, Y. Wu, S. Beghini, G. Montagnoli, F. Scarlassara, R. N. Sagaidak, S. N. Atutov, B. Mai, G. Stancari, L. Tomassetti, E. Mariotti, A. Khanbekyan, and S. Veronesi, Phys. Rev. C **71**, 014609 (2005).

[70] D. Hinde, J. Leigh, J. Newton, W. Galster, and S. Sie, Nucl. Phys. A **385**, 109 (1982).

[71] K. Mahata, S. Kailas, A. Shrivastava, A. Chatterjee, A. Navin, P. Singh, S. Santra, and B. Tomar, Nucl. Phys. A **720**, 209 (2003).

[72] D. G. Sarantites, J. H. Barker, M. L. Halbert, D. C. Hensley, R. A. Dayras, E. Eichler, N. R. Johnson, and S. A. Gronemeyer, Phys. Rev. C **14**, 2138 (1976).

[73] A. Andreyev, D. Bogdanov, V. Chepigin, A. Kabachenko, O. Malyshev, Y. Muzichka, Y. Oganessian, A. Popeko, B. Pustyl-nik, R. Sagaidak, G. Ter-Akopian, and A. Yeremin, Nucl. Phys. A **620**, 229 (1997).

[74] T. Sikkeland, R. J. Silva, A. Ghiorso, and M. J. Nurmia, Phys. Rev. C **1**, 1564 (1970).

[75] D. Vermeulen, H. Clerc, C. Sahm, K. Schmidt, J. Keller, G. Münzenberg, and W. Reisdorf, Z. Phys. A **318**, 157 (1984).

[76] K. T. Lesko, W. Henning, K. E. Rehm, G. Rosner, J. P. Schiffer, G. S. F. Stephans, B. Zeidman, and W. S. Freeman, Phys. Rev. C **34**, 2155 (1986).

[77] D. J. Hinde, R. J. Charity, G. S. Foote, J. R. Leigh, J. O. Newton, S. Ogaza, and A. Chattejee, Nucl. Phys. A **452**, 550 (1986).

[78] G. Mohanto, N. Madhavan, S. Nath, J. Gehlot, I. Mukul, A. Jhingan, T. Varughese, A. Roy, R. K. Bhowmik, I. Mazumdar, D. A. Gothe, P. B. Chavan, J. Sadhukhan, S. Pal, M. Kaur, V. Singh, A. K. Sinha, and V. S. Ramamurthy, Phys. Rev. C **88**, 034606 (2013).

[79] C. R. Morton, A. C. Berriman, R. D. Butt, M. Dasgupta, A. Godley, D. J. Hinde, and J. O. Newton, Phys. Rev. C **62**, 024607 (2000).

[80] S. Gil, F. Hasenbalg, J. E. Testoni, D. Abriola, M. C. Berisso, M. di Tada, A. Etchegoyen, J. O. Fernández Niello, A. J. Pacheco, A. Charlop, A. A. Sonzogni, and R. Vandenbosch, Phys. Rev. C **51**, 1336 (1995).

[81] F. Wolfs, W. Henning, K. Rehm, and J. Schiffer, Phys. Lett. B **196**, 113 (1987).